Наносистеми, наноматеріали, нанотехнології
Nanosistemi, Nanomateriali, Nanotehnologii
2026, т. 24, № 2, сс. 503–518
https://doi.org/10.15407/nnn.24.02.0503

PACS numbers: 51.50.+v, 52.77.Dq, 52.80.Mg, 52.80.Tn, 79.60.Jv, 81.15.Jj, 82.33.Xj

Characteristics and Parameters of a Plasma of a Pulsed Gas-Discharge Reactor with Microparticles of Nickel Flow

O. K. Shuaibov, O. Y. Minya, R. V. Hrytsak, Yu. Yu. Bilak, O. M. Malinin, A. O. Malinina, M. M. Feldiy, O. V. Zubaka, and A. R. Madiar

Uzhhorod National University,
3, Narodna Square,
UA-88000 Uzhhorod, Ukraine

The characteristics of a plasma reactor for generating synchronous flows of nickel micro- and nanoparticles are presented. The reactor operates using an overvoltage nanosecond discharge between nickel electrodes in high-pressure argon ($p = 202.6$ kPa). Nickel vapour is introduced into the plasma through microexplosions of the electrode working-surface inhomogeneities in a strong electric-discharge field continuing 30–40 ns with a current amplitude of up to 300 A and a voltage of up to 25 kV. The following data are analyzed: voltage and current pulse oscillograms, pulse power, and energy contributions to the discharge, plasma spectral characteristics, line emission-intensity dependences on argon pressure, and oscillograms of the most intense spectral lines of the nickel atom. The main excited plasma components of the studied vapour–gas mixtures are identified, and the mechanisms for excitation of nickel atoms in this reactor are examined. The discharge-plasma parameters obtained by numerically solving the Boltzmann equation are presented. The reactor could find application in biomedical engineering for the inactivation of bacteria and harmful, pathogenic viruses.

Представлено характеристики плазмового реактора для ґенерації синхронних потоків мікро- та наночастинок ніклю. Реактор працює з використанням перенапруженого наносекундного розряду між ніклевими електродами в арґоні високого тиску ($p = 202{,}6$ кПа). Пари ніклю вводилися у плазму шляхом мікровибухів неоднорідностей робочої поверхні електрод у сильному полі електричного розряду тривалістю у 30–40 нс з амплітудою струму до 300 А і напругою до 25 кВ. Було проаналізовано наступні дані: осцилограми імпульсів напруги та струму, внески потужности й енергії імпульсу в розряд, спектральні характеристики плазми, залежності інтенсивности лінійного випромінювання від тиску арґону й осцилограми найінтенсивніших спектральних ліній атома Ні-

клю. Було ідентифіковано основні збуджені плазмові компоненти досліджуваних парогазових сумішей і досліджено механізми збудження атомів Ніклю в цьому реакторі. Представлено параметри плазми розряду, одержані шляхом чисельного розв'язання Больцманнового рівняння. Реактор може знайти застосування в біомедичній інженерії для інактивації бактерій і шкідливих, патогенних вірусів.

Key words: electric discharge, plasma, argon, nanonickel, nanoparticles.

Ключові слова: електричний розряд, плазма, арґон, нанонікель, наночастинки.

(Received 4 February, 2026)

1. INTRODUCTION

The widespread use of metal-based inorganic nanoparticles in medicine, biology, and ecology has stimulated research into the synthesis methods and characteristics of such nanoparticles. Currently, metal oxide nanoparticles ZnO, TiO_2, SiO_2, Fe_2O_3 have been most thoroughly studied [1, 2]. However, it is important to expand the class of nanoparticles promising for biomedical application to include metal nanoparticles (W) [3, 4], (Cu) [5], and (Zn) [6, 7].

Among metal nanoparticles, the synthesis methods, characteristics, parameters, and biomedical applications of nanoparticles of noble and some other metals Ag, Au, Pt, Zn, *etc.* have been most extensively studied [8–11]. Thus, more than 20 000 scientific articles, monographs, and conference proceedings have been published on the topic of silver nanoparticles. The conditions for synthesizing nanoparticles of other metals and their characteristics, including nickel, remain less studied.

Nanonickel has a number of important technical applications related to its excellent ferromagnetic properties, monoclinic anisotropy, high coercivity, and significant chemical stability [12]. Therefore, various nanonickel synthesis methods are important for engineering practice and are constantly being improved.

In addition to chemical and biological methods for synthesizing nanonickel, physical methods are also important, allowing the production of thin films and finely dispersed nickel powder. Nickel nanoparticles are synthesized, using laser plasma [13], high-frequency low-pressure discharge (magnetron) [14], and spark discharge between nickel electrodes at an interelectrode distance of 8–15 mm [15].

In Ref. [16], the results of a study of nickel-atom sputtering from the surface of pulsed discharge electrodes using laser-induced fluorescence are presented. This is important for understanding the

operating resilience of electrodes at a fixed distance between them.

When the distance between metal electrodes in a nanosecond spark discharge is reduced to 1–3 mm, it ignites and burns in an overvoltage mode and is characterized by increased spatial homogeneity. In this case, runaway electrons and their accompanying x-ray radiation play the role of a preliminary ionization system of the interelectrode gap [17]. Conditions for the synthesis of tungsten and zinc nanoparticles in such a discharge were studied in Refs. [4, 7].

Some electrical and spectral characteristics of the overvoltage nanosecond discharge (OVND) between nickel electrodes in argon at atmospheric pressure, suitable for the synthesis of nanonickel, are presented in Ref. [18]. In OVND, the introduction of electrode material (metal) vapours occurs during the formation of ectons [19], which are formed by the bulging of nanoscale asperities on the electrode surface in the strong electric field of the OVND. This method of introducing vapours, even of refractory metals, allows OVND ignition in dielectric cells with wall temperatures close to room temperature.

As follows from the above studies, nanonickel synthesis in OVND may have several advantages, as magnetron discharge systems are quite expensive and require the creation of a high vacuum; laser methods also require the implementation of expensive equipment and cannot ensure the synthesis of powders on a large scale.

Currently, the conditions for synthesizing nanonickel in OVND between nickel electrodes in a high-pressure inert gas environment are being studied.

This article presents the results of a study of the characteristics and parameters of a pulsed plasma gas reactor based on the OVND between nickel electrodes in argon. This reactor can be used to generate a beam of nickel microparticles and a plasma stream of UV radiation, or to synthesize thin nickel films on a solid substrate placed near the electrode system. The generated microparticle beams can be applied in biomedical engineering and microbiology.

2. EXPERIMENTAL TECHNIQUE

The characteristics of the OVND between electrodes with nickel in an argon medium were measured in a dielectric discharge chamber with a distance between the electrodes $d = 2$ mm.

To ignite the OVND, high voltage pulses with a frequency of 100–150 ns, amplitude of ±(20–40) kV and a frequency of voltage pulses of $f = 80$–1000 Hz were applied to the electrodes of the discharge chamber.

The discharge chamber was pumped up with a forevacuum pump to an excessive pressure of 5–10 Pa, and then argon was released

into the chamber until the required pressure was reached. The diameter of the cylindrical nickel electrodes is of 5 mm, and the radius of rounding of their working end surface is equal to 3 mm.

A more detailed description of the research methodology for the experimental setup is given in Ref. [20].

3. ELECTRICAL AND OPTICAL PROPERTIES OF THE OVND

At atmospheric argon pressure and an interelectrode distance of $d = 2$ mm, the OVND had the appearance of a bright central region approximately 2 mm in diameter.

The voltage, current, and pulse power waveforms for the OVND in the gas–vapour Ar–Ni mixture are shown in Fig. 1.

The voltage and current waveforms exhibited decaying oscillations continuing approximately 20–40 ns. The total duration of the gap-voltage and discharge-current oscillations was of 450–500 ns.

At a pressure of $p(\mathrm{Ar}) = 13.3$ kPa, the maximum amplitude of the first positive half-wave of the voltage was of 7.5 kV. At the decline of the first positive half-wave of the voltage, a current pulse with a positive amplitude of 200 A was formed. The main maximum of the pulse power reached 1 MW, the energy contribution to the plasma per one discharge pulse was of 79.2 mJ. At $p(\mathrm{Ar}) = 202.6$ kPa, the first positive voltage maximum increased to 17 kV. The first positive current maximum had an amplitude of up to 200 A, and the amplitudes of the next two current maxima increased to 200 A. This behaviour of the voltage and current waveforms may be due to the mismatch of the output resistance of the high-voltage modulator with the OVND plasma, which played the role of a load.

The pulse power of the OVND reached 2.5 MW with an energy

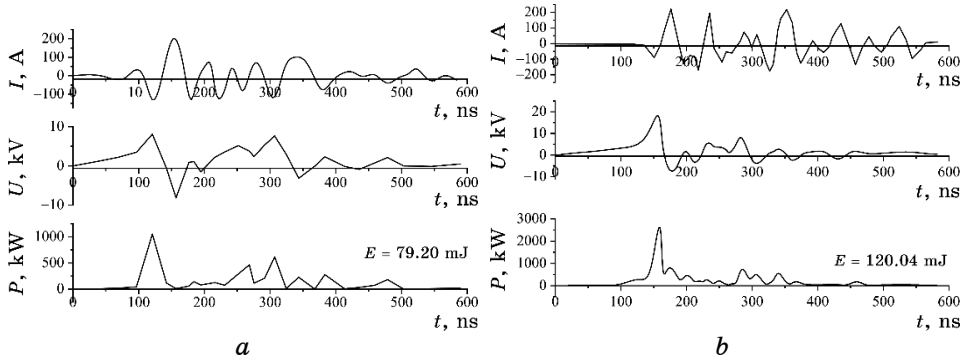

Fig. 1. Oscillograms of current, voltage and pulse power of the OVND between nickel electrodes at argon pressures of 13.3 kPa (*a*) and 202.6 kPa (*b*).

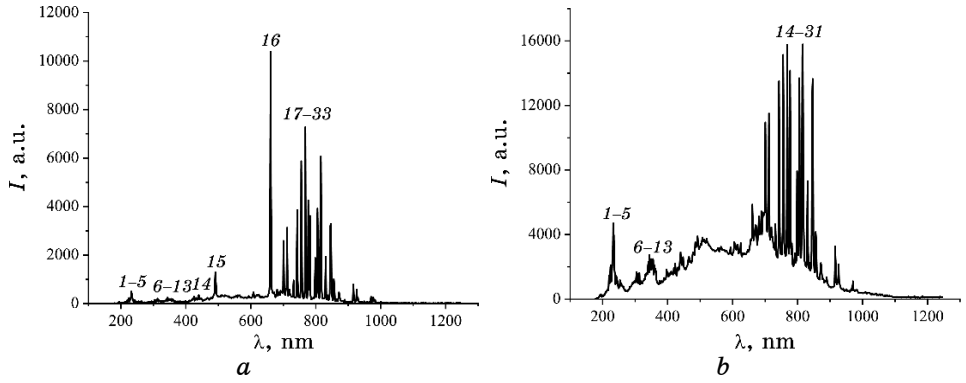

Fig. 2. Radiation spectrum of the OVND between nickel electrodes at: (*a*) p(Ar) = 13.3 kPa, (*b*) 202.6 kPa (d = 2 mm, f = 1000 Hz).

contribution of one OVND-discharge pulse of 120 mJ.

The emission spectra of the OVND ignited between nickel electrodes at different argon pressures are shown in Fig. 2, and the results of its identification of the spectrum shown in Fig. 2, *b* are in Table 1. When deciphering the plasma emission spectrum, reference books [21, 22] were used.

All spectral lines are located on the recombination continuum of argon [23, 24], the brightness of which increased with increasing argon pressure.

When the argon pressure was reduced in the range from 202.3 to 13.3 kPa and the voltage-pulse repetition frequency was reduced from 1000 to 80 Hz, the OVND emission spectra in gas–vapour Ar–Ni mixtures remained practically unchanged, only the intensity of all spectral lines decreased.

In addition to the spectral lines of Ni–I and Ar–I in the UV and near-infrared ranges, in the visible part of the spectrum, a rather intense line of the hydrogen atom, 656.3 nm H_α, was also observed. The appearance of this line in the emission spectra of the OVND is due to small impurities of water vapour in the residual gas after pumping out the chamber, and water vapour in a small amount was also present in argon.

This is reflected in Figs. 3–5, from which it can be seen that, with an increase in the argon pressure from 13.3 to 202.6 kPa, the intensity of the spectral lines in the spectral UVC range 224.5–232.0 nm Ni–I increased from 50 to 450 rel. units, the intensity of the Ni–I lines in the UVA range 338.1, 341.5, 345.6, 352.5 nm increased approximately from 50 to 250 rel. units. The intensity of the argon spectral lines, at the same time, increased from 3000 to 15 000 rel. units.

TABLE 1. Results of decoding the emission spectrum of the OVND plasma based on the gas–vapour Ar–Ni mixture (shown in Fig. 2, *b*).

No.	λ_{table}, nm	$I_{exp.}$, a.u.	Object	E_{low}, eV	E_{upper}, eV	Term_{low}	Term_{upper}
1	219.7	1471	Ni–I	0.21	5.85	$3d^9(^2D)4s\ ^3D_1$	$3d^8(^3P)4s4p(^3P)\ ^3P_1$
2	224.5	2088	Ni–I	0.109	5.631	$3d^9(^2D)4s\ ^3D_2$	$3d^8(^3F)4s4p(^1P)\ ^3F^\circ_2$
3	232.0	4711	Ni–I	0	5.34	$3d^8(^3F)4s^2\ ^3F_4$	$3d^8(^3F)4s4p(^1P)\ ^3G_5$
4	241.9	1433	Ni–I	0.165	5.28	$3d^8(^3F)4s^2\ ^3F_3$	$3d^8(^1D)4s4p\ (^3P)\ ^3D_2$
5	300.2	1684	Ni–I	0.025	4.15	$3d^9(^2D)4s\ ^3D_3$	$3d^8(^3F)4s4p\ (^3P)\ ^3D_3$
6	305.1	1572	Ni–I	0.025	4.088	$3d^9(^2D)4s\ ^3D_3$	$3d^8(^3F)4s4p(^3P)\ ^3F_4$
7	310.2	1624	Ni–I	0.109	4.105	$3d^9(^2D)4s^3D_2$	$3d^8(^3F)4s4p(^3P)^3F_3$
8	338.1	2303	Ni–I	0.42	4.089	$3d^9(^2D)4s^1D_2$	$3d^9(^2D)4P\ ^1P_1$
9	341.5	2730	Ni–I	0.025	3.6551	$3d^9(^2D)4s^3D_3$	$3d^9(^2D)4P\ ^3F_4$
10	345.8	2484	Ni–I	0.21	3.796	$3d^9(^2D)4s\ ^3D_1$	$3d^9(^2D)4P\ ^3F_2$
11	352.5	2482	Ni–I	0.025	3.542	$3d^9(^2D)4s\ ^3D_3$	$3d^9(^2D)4P\ ^3P_2$
12	356.6	2078	Ni–I	0.422	3.898	$3d^9(^2D)4s\ ^1D_2$	$3d^9(^2D)4P\ ^1D_2$
13	361.9	1886	Ni–I	0.422	3.847	$3d^9(^2D)4s\ ^1D_2$	$3d^9(^2D)4P^1F_3$
14	656.3	5851	H_α	10.20	12.09	$2p\ ^2P^0_{1/2}$	$3d\ ^2D_{3/2}$
15	696.5	10950	Ar–I	11.54	13.32	$3s^23p^5(^2P_{3/2})4s\ ^2[3/2]_2$	$3s^23p^5(^2P_{1/2})4p\ ^2[1/2]_1$
16	706.7	11513	Ar–I	11.54	13.30	$3s^23p^5(^2P_{3/2})4s\ ^2[3/2]_2$	$3s^23p^5(^2P_{1/2})4p\ ^2[3/2]_2$
17	727.3	3451	Ar–I	11.62	13.32	$3s^23p^5(^2P_{3/2})4s\ ^2[3/2]_1$	$3s^23p^5(^2P_{1/2})4p\ ^2[1/2]_1$
18	731.6	4658	Ar–I	13.32	15.02	$3s^23p^5(^2P_{1/2})4P\ ^2[1/2]_1$	$3s^23p^5(^2P_{1/2})6s\ ^2[1/2]_1$
19	738.4	13506	Ar–I	11.62	13.30	$3s^23p^5(^2P_{3/2})4s\ ^2[3/2]_1$	$3s^23p^5(^2P_{1/2})4p\ ^2[3/2]_2$
20	751.5	15143	Ar–I	11.62	13.27	$3s^23p^5(^2P_{3/2})4s\ ^2[3/2]_1$	$3s^23p^5(^2P_{3/2})4p\ ^2[1/2]_0$
21	763.5	15745	Ar–I	11.54	13.17	$3s^23p^5(^2P_{3/2})4s\ ^2[3/2]_2$	$3s^23p^5(^2P_{3/2})4p\ ^2[3/2]_2$
22	772.4	14145	Ar–I	11.72	13.32	$3s^23p^5(^2P_{1/2})4s\ ^2[1/2]_0$	$3s^23p^5(^2P_{1/2})4p\ ^2[1/2]_1$
23	794.8	7931	Ar–I	11.72	13.28	$3s^23p^5(^2P_{1/2})4s\ ^2[1/2]_0$	$3s^23p^5(^2P_{1/2})4p\ ^2[3/2]_1$
24	801.5	13685	Ar–I	11.54	13.09	$3s^23p^5(^2P_{3/2})4s\ ^2[3/2]_2$	$3s^23p^5(^2P_{3/2})4p\ ^2[5/2]_2$
25	811.5	15784	Ar–I	11.54	13.07	$3s^23p^5(^2P_{3/2})4s\ ^2[3/2]_2$	$3s^23p^5(^2P_{3/2})4p\ ^2[5/2]_3$
26	826.5	7321	Ar–I	11.82	13.32	$3s^23p^5(^2P_{1/2})4s\ ^2[1/2]_1$	$3s^23p^5(^2P_{1/2})4p\ ^2[1/2]_1$
27	842.5	13651	Ar–I	11.62	13.09	$3s^23p^5(^2P_{3/2})4s\ ^2[3/2]_1$	$3s^23p^5(^2P_{3/2})4p\ ^2[5/2]_2$
28	852.1	4152	Ar–I	11.82	13.28	$3s^23p^5(^2P_{1/2})4s\ ^2[1/2]_1$	$3s^23p^5(^2P_{1/2})4p\ ^2[3/2]_1$
29	912.3	3275	Ar–I	11.54	12.90	$3s^23p^5(^2P_{3/2})4s\ ^2[3/2]_2$	$3s^23p^5(^2P_{3/2})4p\ ^2[1/2]_1$
30	922.4	2165	Ar–I	11.82	13.17	$3s^23p^5(^2P_{1/2})4s\ ^2[1/2]_1$	$3s^23p^5(^2P_{3/2})4p\ ^2[3/2]_2$
31	965.77	1115	Ar–I	11.62	12.90	$3s^23p^5(^2P_{3/2})4s\ ^2[3/2]_1$	$3s^23p^5(^2P_{3/2})4p\ ^2[1/2]_1$

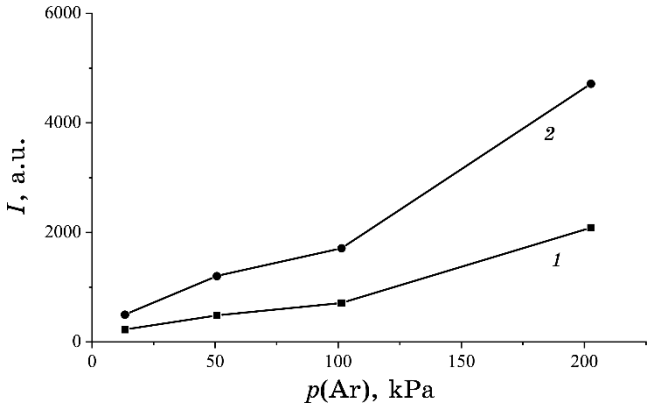

Fig. 3. Dependence of the intensity of the Ni–I lines on the argon pressure in an overvoltage nanosecond discharge between nickel electrodes ($f = 1000$ Hz, $d = 2$ mm): *1*—224.45 nm (Ni–I), *2*—232.003 nm (Ni–I).

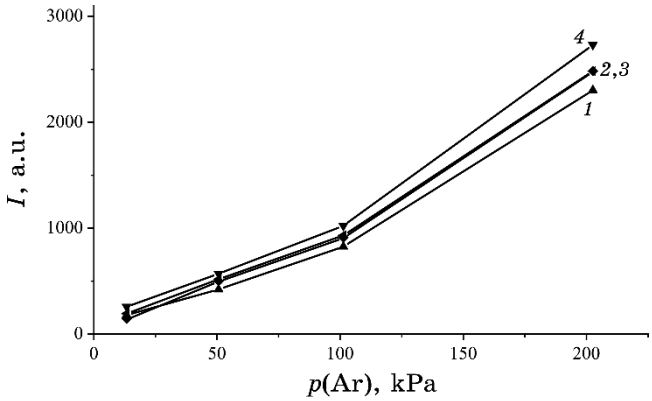

Fig. 4. Dependence of the intensity of the Ni–I lines on the argon pressure in an overvoltage nanosecond discharge between nickel electrodes ($f = 1000$ Hz, $d = 2$ mm): *1*—338.05 nm, *2*—352.45 nm, *3*—345.84 nm, *4*—341.476 nm.

It should be noted that the increase in the intensity of the 842.5 nm Ar–I spectral line on the argon pressure occurred according to a linear law, and the intensity of the 763.5 nm, 811.5 nm Ar–I lines reached saturation with increasing argon pressure. The lower energy levels for the spectral lines are the metastable Ar–I levels, and for the line with $\lambda = 842.5$ nm, Ar–I is the resonance level [25]. With increasing argon pressure, the population of the metastable Ar–I levels increases, and the intensities of the 763.5 nm, 811.5 nm Ar–I lines reach saturation.

Figure 6 shows the oscillograms of the characteristic spectral

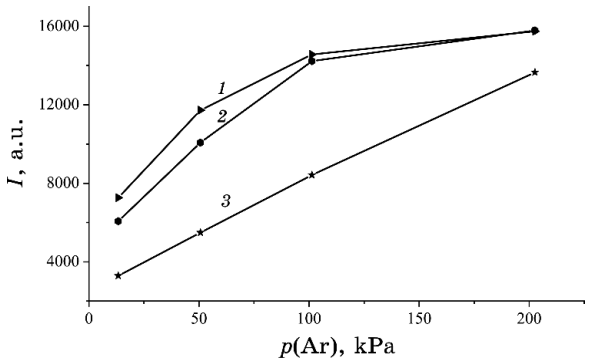

Fig. 5. Dependence of the intensity of the Ar–I lines on the argon pressure in an overvoltage nanosecond discharge between nickel electrodes ($f = 1000$ Hz, $d = 2$ mm): *1*—763.51 nm, *2*—811.53 nm, *3*—842.46 nm.

lines of the nickel atom and the current oscillograms at an argon pressure of 101.3 kPa.

All the oscillograms of the glow at the Ni–I transitions are located in the near afterglow of the first maximum of the discharge current. This may be due to the recombination mechanism of the population of the upper energy levels of the nickel atom lines, which decay with radiation in the UV-wavelength region. The practical absence of radiation of nickel atoms from the current maxima that develops in time after the first (main) current maximum indicates the contraction of the discharge in this time interval.

4. PLASMA PARAMETERS

The discharge-plasma parameters in the argon–nickel mixture vapour at atmospheric pressure (component ratio 202 kPa : 300 Pa = $= p(\mathrm{Ar}) : p(\mathrm{Ni})$) were determined numerically and calculated as total integrals of the electron energy distribution functions (EEDFs). The EEDFs were found numerically by solving the kinetic Boltzmann equation within the binomial approximation [26]. The EEDFs were calculated using the program presented in Ref. [27].

Based on the obtained EEDFs, a number of plasma parameters were determined depending on the magnitude of the reduced electric field (the ratio of the electric field strength (E) to the total concentration of Ar atoms and nickel vapour impurities (N)). The range of E/N-parameter changes is of 1–200 Td ($1 \cdot 10^{-17}$–$2 \cdot 10^{-15}$ V·cm^2) included the values of E/N parameter, which were implemented in the experiment. These values of E/N parameter were of 143 Td and 61 Td for times of 150 ns and 275 ns from the beginning of the discharge ignition. The following processes are taken

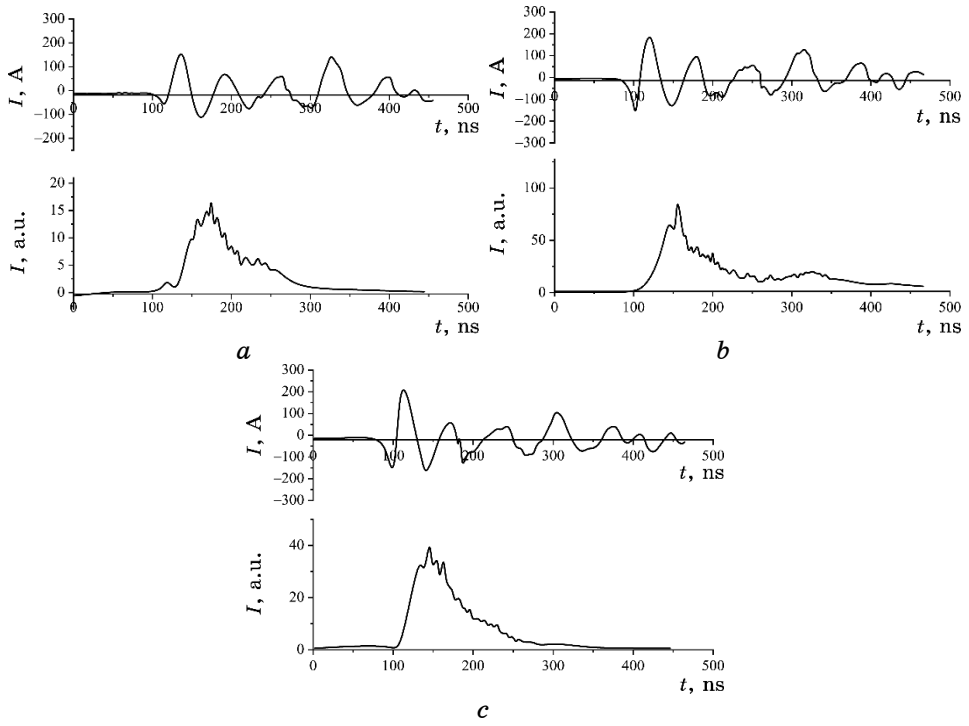

Fig. 6. Oscillograms of current pulses and the glow of spectral lines of the Ni atom at $p(\mathrm{Ar}) = 101.3$ kPa: *a*—305.08 nm Ni–I, *b*—345.84 nm Ni–I, *c*—356.63 nm Ni–I.

into account in the integral of electron collisions with atoms: elastic and superelastic scattering of electrons on Ni and Ar atoms, excitation by electrons of energy levels of the Ni atom, from which radiation occurs at wavelengths of $\lambda = 231.096$ nm, 233.749 nm, 305.082 nm, $339 \cdot 10^4$ nm, ionization of the Ni atom, which has a threshold energy of 7.6 eV, excitation of the energy level of the Ar atom (threshold energy of 11.50 eV), ionization of the Ar atom (threshold energy of 15.80 eV), and electron–electron and electron–ion collisions were also taken into account [27–30].

Figure 7 shows the dependence of the mean electron energy in the plasma in the mixture of argon with nickel vapour $p(\mathrm{Ar}) : p(\mathrm{Ni}) = 202000\ \mathrm{Pa} : 300\ \mathrm{Pa}$ at a total pressure $p = 202300$ Pa on the reduced electric-field strength. The mean electron energy of the discharge for the vapour–gas mixture $p(\mathrm{Ni}) : p(\mathrm{Ar}) = 300\ \mathrm{Pa} : 202000\ \mathrm{Pa}$ increased from 1.805 to 7.854 eV with an increase in the reduced electric-field strength from 1 Td to 200 Td (Fig. 7). At the same time, a pattern of increased rate of its change was observed in the range of 1–30 Td. For times of 150 ns and 275 ns from the beginning of the

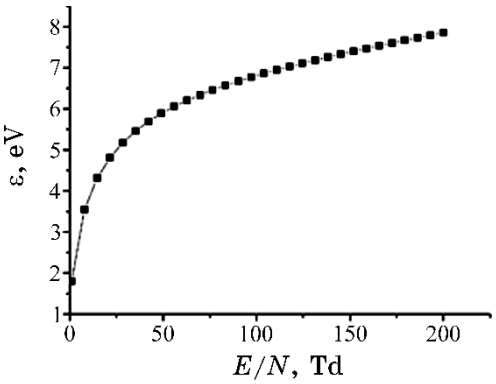

Fig. 7. Dependence of the mean electron energy in the plasma of the vapour–gas mixture $p(\mathrm{Ni}) : p(\mathrm{Ar}) = 300\ \mathrm{Pa} : 202000\ \mathrm{Pa}$ on the reduced electric-field strength.

TABLE 2. Transport characteristics of electrons (mean energies (ε), temperature (T), drift velocity ($V_{dr.}$) and electron concentrations (N_e)) in a discharge in the Ni–Ar mixture vapour at a component ratio of 300 : 202000 for times of 150 ns and 275 ns from the beginning of the discharge ignition.

τ, ns	E/N, Td	Mixture: Ni–Ar = 300 Pa–101000 Pa			
		ε, eV	T, K	$V_{dr.}$, m/s	N_e, m^{-3}
150	143	7.33	85051	$1.1 \cdot 10^5$	$2.61 \cdot 10^{20}$
275	61	6.20	71966	$5.7 \cdot 10^4$	$3.36 \cdot 10^{20}$

discharge ignition, the mean energies had values of 7.23 and 6.20 eV, respectively, which corresponded to their plasma temperatures of 71966 K and 85051 K (Table 2).

The electron drift velocity values were of $2.61 \cdot 10^5$ m/s for a plasma field strength of $7 \cdot 10^6$ V/m and $3.36 \cdot 10^4$ m/s for a plasma field strength of $3 \cdot 10^6$ V/m, which was reached at a time of 150 ns from the beginning of the breakdown of the interelectrode gap (the value of the voltage pulse amplitude was 14 000 V; Fig. 1) and at a time of 275 ns from the beginning of the breakdown of the interelectrode gap, respectively. The electron concentration value is of $2.61 \cdot 10^{20}$ m^{-3}–$3.36 \cdot 10^{20}$ m^{-3} at a current density of $(4.59–3.06) \cdot 10^6$ $\mathrm{A/m}^2$ on the electrode surface ($S = 0.196 \cdot 10^{-4}$ m^2) for a reduced electric-field strength $E/N = 143$ Td, which existed in the discharge gap at a time of 150 ns and for a reduced electric-field strength $E/N = 61$ Td, which existed in the discharge gap at a time of 275 ns.

Figure 8 shows the dependence of the specific discharge-power losses in the processes of electron collisions with Ni and Ar atoms in the plasma in the mixture $p(\mathrm{Ar}) : p(\mathrm{Ni}) = 202000\ \mathrm{Pa} : 300\ \mathrm{Pa}$ at a

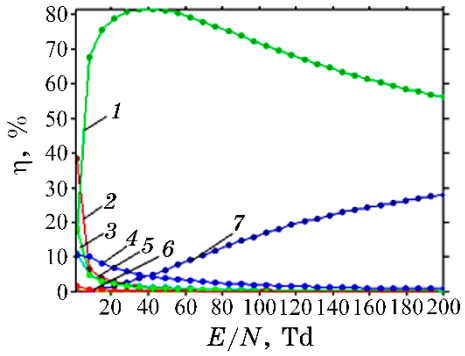

Fig. 8. Dependence of specific discharge power losses (η) in the processes of electron collisions with Ni and Ar atoms on the parameter E/N in the plasma for the mixture p(Ar) : p(Ni) = 202000 Pa : 300 Pa: *1*—excitation of the state of Ar atoms (E = 11.50 eV); *2*—elastic scattering of electrons on Ar atoms; *3*—excitation of the energy level of Ni atoms (λ = 305.082 nm); *4*—ionization of Ni atoms (threshold energy of 7.60 eV); *5*—excitation of the energy level of Ni atoms (λ = 231.096 nm); *6*—excitation of the energy level of Ni atoms (λ = 339.104 nm); *7*—ionization of Ar atoms (threshold energy of 15.8 eV).

total pressure p = 202300 Pa on the parameter E/N.

Specific discharge-power losses in the Ni–Ar mixture vapour (argon : nickel = 202000 Pa : 300 Pa) due to inelastic processes of electron collisions with the components of the mixture for a reduced electric-field strength of 143 Td are maximum for excitation of the energy level of Ar atoms (threshold energy of 11.50 eV) and ionization of Ar atoms with a threshold energy of 15.8 eV (Fig. 8, curves *1* and *7*) and reach 63.5% and 22.8%, respectively. Moreover, for reduced field strength E/N = 61 Td, which occurred at 275 ns from the beginning of the breakdown of the plasma gap, they did not exceed 79.2% and 9.1%, respectively.

For Ni atoms, the maximum specific discharge-power losses of 18.3% were observed for the energy transition $3d^9(^2D)4s\ ^3D$–$3d^8(^3F)4s4p(^3P_0)\ ^3F_0$, in which radiation occurs at a wavelength of 305.082 nm at a reduced electric-field strength of 1 Td, and for reduced electric field strengths of 143 Td and 61 Td, they are of 0.02% and 0.07% (Fig. 8, curve *3*). With an increase in the E/N parameter to 200 Td, the specific discharge-power losses in the mixture decrease except for the ionization of Ar atoms (Fig. 8, curve *7*). The rate of increase and decrease of discharge-power losses in the processes of excitation of electronic states and ionization and its magnitude are related to the nature of the dependence of the effective cross-sections of inelastic processes of collisions of electrons with mixture components on the energies of electrons, their absolute values, and on the dependence of the electron distribution

function on the value of the reduced field strength and the value of the threshold energy of the process [30].

The total specific power-discharge losses in the inelastic processes of collisions of electrons with Ar and Ni atoms were of $1.426 \cdot 10^{-14}$ eV·m^3/s and $3.411 \cdot 10^{-15}$ eV·m^3/s for $E/N = 143$ Td and 61 Td, respectively, and they were approximately three orders of magnitude larger compared to elastic losses (Fig. 9, Table 3).

Figure 10 presents the results of numerical calculation of the dependence of the rate constants of electron collisions with Ar and Ni atoms on the parameter E/N in the Ar–Ni mixture vapour for the ratio of partial pressures in the mixture of 202000 Pa : 300 Pa at a total pressure of the mixture $p = 202300$ Pa. The rate constants vary in the range of values $k \approx 2.2 \cdot 10^{-23}$–$1.6 \cdot 10^{-13}$ m^3/s, which is associated with the values of the absolute effective cross-sections of the corresponding processes. For Ni atoms (Fig. 6), they vary in the range of $1.9 \cdot 10^{-17}$–$2.1 \cdot 10^{-14}$ m^3/s for the reduced electric-field strength $E/N = 1$–200 Td.

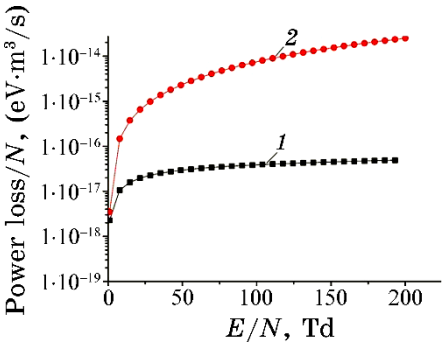

Fig. 9. Dependence of the specific power of the discharge in elastic (*1*) and inelastic (*2*) processes on the reduced electric-field strength for the mixture p(Ni) : p(Ar) = 300 Pa : 202000 Pa.

TABLE 3. The value of the specific power of the discharge losses in elastic and inelastic processes of collisions of electrons with Ar and Ni atoms on the reduced electric-field strength in the plasma of the vapour–gas mixture p(Ar) : p(Ni) = 202000 Pa : 300 Pa at a total pressure of 202300 Pa for reduced electric-field strengths of 143 Td and 61 Td.

Mixture: Ni–Ar = 300 Pa–101000 Pa		
E/N, Td	Elastic processes, Power/N, eV·m^3/s	Inelastic processes, Power/N, eV·m^3/s
143	$0.4423 \cdot 10^{-16}$	$0.1426 \cdot 10^{-13}$
61	$0.3243 \cdot 10^{-16}$	$0.3411 \cdot 10^{-14}$

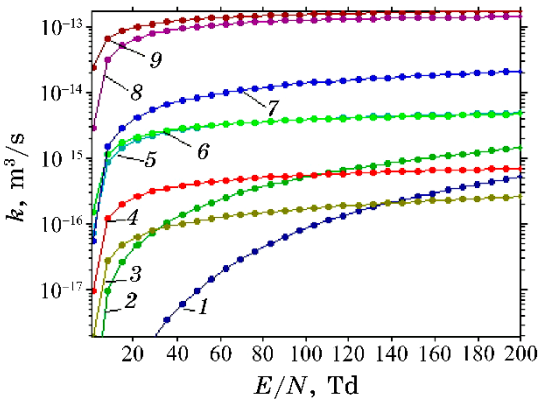

Fig. 10. Dependences of the rate constants of collisions of electrons with Ni and Ar atoms on the parameter E/N in a discharge in the gas–vapour mixture Ar : Ni = 202000 Pa : 300 Pa: *1*—ionization of Ar atoms (E = 15.80 eV); *2*—excitation of the state of Ar atoms (E = 11.50 eV); *3*—excitation of the state of Ni atoms (λ = 233.749 nm); *4*—excitation of the state of Ni atoms (λ = 339.104 nm); *5*—excitation of the state of Ni atoms (λ = 231.096 nm); *6*—excitation of the state of Ni atoms (λ = 305.082 nm); *7*—elastic scattering of electrons on Ni atoms; *8*—elastic scattering of electrons on Ar atoms; *9*—ionization of Ni atoms (threshold energy of 7.6 eV).

TABLE 4. Rate constants of radiation excitation (K_{Ni*}) and ionization (k_{Ni^+}) of Ni atoms by electrons in the Ni–Ar mixture vapour at a ratio of 300 Pa : 202000 Pa.

E/N, Td	$K_{Ni*}\cdot10^{+14}$, m^3/s λ = 305.082 nm	$K_{Ni*}\cdot10^{+14}$, m^3/s λ = 231.096nm	$K_{Ni*}\cdot10^{+15}$, m^3/s λ = 233.749nm	$K_{Ni*}\cdot10^{+15}$, m^3/s λ = 339.304 nm	$k_{Ni^+}\cdot10^{+13}$, m^3/s
143	0.4260	0.4389	0.2137	0.6426	0.1734
61	0.3311	0.3249	0.1300	0.4823	0.1000

For the reduced electric-field strength E/N = 143 Td, which existed in the discharge gap at the time of 150 ns, and for the reduced electric-field strength E/N = 61 Td, which existed in the discharge gap at the time of 275 ns, the excitation rate constants of the spectral line of 305.082 nm (for the energy transition $3d^9(2D)4s\ ^3D–3d^8(^3F)4s4p(^3P_0)\ ^3F_0$) had the values of $0.4260\cdot10^{-14}$ m^3/s and $0.3311\cdot10^{-14}$ m^3/s, respectively (Table 4).

5. CONCLUSIONS

As shown, in the gas–arc Ar–Ni mixture at atmospheric pressure between the electrodes of nickel, a homogeneous discharge in the form of a ball with a diameter of 2 mm was ignited (at $d = 2$ mm and $f = 1000$ Hz). The first positive maximum of the current pulse had an amplitude of up to 200 A, the corresponding maximum of the voltage pulse had an amplitude of 17 kV and had a duration of 30–40 ns; the maximum pulse power was of 2.5 MW, and the magnitude of the energy contribution to the plasma per discharge pulse reached 120 mJ.

The study of the spectral characteristics of the OVND showed that the plasma is a source of UV radiation in the transitions of the Ni atom in the spectral region of 210–350 nm. Reducing the pressure of the gas–vapour Ar–Ni mixture from 202.6 to 13.3 kPa and the frequency from 1000 to 80 Hz led to a significant decrease in the intensity of all spectral lines and the brightness of the recombination continuum; against the background of which, they were observed. The nature of the oscillograms of the glow of the spectral lines of the Ni atom indicates a significant probability of the implementation of the recombination mechanism of population of the upper energy levels of the Ni atom.

Studies of the transport characteristics of electrons and the power of discharge losses in the elastic and inelastic processes of electron collisions with the components of the vapour–gas Ni–Ar mixture established that the mean energy of discharge electrons for the vapour–gas mixture $p(\mathrm{Ni}) : p(\mathrm{Ar}) = 300$ Pa : 202000 Pa increased from 1.806 to 7.854 eV with an increase in the reduced electric-field strength from 1 to 200 Td. For times of 150 ns and 275 ns from the beginning of the discharge ignition, the mean energies had values of 7.33 eV and 6.20 eV, respectively, which corresponded to their plasma temperatures of 85051 K and 71966 K. The discharge-power losses for the elastic and inelastic processes of electron collisions with components of vapour–gas mixtures also increase with an increase in the reduced electric-field strength within 1–200 Td. They had larger values for inelastic processes of electron collisions with components of the vapour–gas mixture and were approximately three orders of magnitude higher in comparison with elastic losses. For reduced electric-field strength of 143 Td, the value of the discharge-power loss for inelastic processes was of $0.1426 \cdot 10^{-13}$ eV·m^3/s. An increase in the value of the excitation-rate constants of the spectral lines of the Ni atom with an increase in the reduced electric-field strength is also characteristic. For the reduced electric-field strength $E/N = 143$ Td, which existed in the discharge gap at the time of 150 ns, and for the reduced electric-field strength

$E/N = 61$ Td, which existed in the discharge gap at the time of 275 ns, the excitation-rate constants of the upper Ni term ($3d^8(^3F)4s^2\,^3F$), from which radiation at the wavelength $\lambda = 231.096$ nm comes, had the values of $0.4389 \cdot 10^{-14}$ m^3/s and $0.3249 \cdot 10^{-14}$ m^3/s, respectively, that ensures its sufficient intensity in the discharge for use in diagnostics and deposition of the corresponding films.

REFERENCES

1. S. I. Tsekhmistrenko, V. S. Bityuts'kiy, O. S. Tsekhmistrenko, O. A. Demchenko, N. O. Timoshok, and O. M. Mel'nichenko, *Ehkologichni Biotekhnologiï 'Zelenogo' Syntezu Nanochastynok Metaliv, Oksydiv Metaliv, Metaloyidiv ta Yikh Vykorystannya* [Environmental Biotechnology of 'Green' Synthesis of Nanoparticles of Metals, Metal Oxides, Metalloids and Their Use] (Bila Tserkva: Naukove Vydannya: 2022) (in Ukrainian).
2. I. S. Chekman, *Nanonauka: Medyko-Biologichni Osnovy* [Nanoscience: Biomedical Fundamentals] (Kyiv: Vydavnychyy Dim 'Medkniga': 2017) (in Ukrainian).
3. Dongyoon Shin, Hyun-Woo Shim, Basudev Swain, Kyung-Soo Park, and Chan-Gi Lee, *Korean J. Met. Mater.*, **58**, No. 11: 798 (2020); http://dx.doi.org/10.3365/KJMM.2020.58.11.798
4. O. K. Shuaibov, R. V. Gritsak, O. Y. Minya, Z. T. Gomoki, and M. I. Vatrala, *Nanosistemi, Nanomateriali, Nanotehnologii*, **23**, Iss. 1: 123 (2025); http://dx.doi.org/10.15407/nnn.23.01.0123
5. J. Kousal, A. Shelemin, M. Schwartzkopf, O. Polonskyi, J. Hanuš, P. Solař, M. Vaidulych, D. Nikitin, P. Pleskunov, Z. Krtouš, T. Strunskus, F. Faupel, S. V. Roth, H. Biederman, and A. Choukourov, *Nanoscale*, **10**: 18275 (2018); https://doi.org/10.1039/C8NR06155F
6. I. S. Chekman, Z. R. Ul'berg, A. D. Rudenko, Yu. V. Marushko et al., *Ukr. Med. Chasopys*, **2**, No. 94: 42 (2013).
7. O. K. Shuaibov, O. Y. Minya, R. V. Hrytsak, A. O. Malinina, and O. M. Malinin, *Journal of Nano- and Electronic Physics*, **17**, No. 1: 01021 (2025); https://doi.org/10.21272/jnep.17(1).01021
8. Khadijah A. Altammar, *Front. Microbiol.*, **14**: 1155662 (2023); https://doi.org/10.3389/fmicb.2023.1155622
9. Priyanka Singh, Santosh Pandit, Sri Renukadevi Balusamy, Mukil Madhusudanan, Hina Singh, H. Mohamed Amsath Haseef, and Ivan Mijakovic, *Advanced Healthcare Materials*, **14**, No. 4: e2403059 (2025); https://doi.org/10.1002/adhm.202403059
10. Md. Hazrat Ali, Md. Abul Kalam Azad, K. A. Khan, Md. Obaidur Rahman, Unesco Chakma, and Ajoy Kumer, *ACS Omega*, **8**, Iss. 31: 28133 (2023); https://doi.org/10.1021/acsomega.3c01261
11. Xi-Feng Zhang, Zhi-Cuo Lin, Wei Shen, and Sagiliyandi Guru Nathan, *Int. Journ. of Mol. Sciences*, **17**, No. 9: 1534 (2016); https://doi.org/10.3390/ijms17091534
12. Nuru-Deen Jaji, Hooi Ling Lee, Mohd Hazwan Hussin, Hazizan Md Akil, Muhammad Razlan Zakaria, and Muhammad Bisyrul Hafi Othman, *Nanotechnology Reviews*, **9**: 1456 (2020); https://doi.org/10.1515/ntrev-

2020-0109
13. Amir Reza Sadrolhosseini, A. S. M. Noor, Kamyar Shameli, Alireza Kharazmi, N. M. Huang, and M. A. Mahdi, *Journal of Nanomaterials*, **986764**: 9 (2013); https://doi.org/10.1155/2013/986764
14. Slamet Widodo, *International Journal of Innovative Science, Engineering & Technology*, **2**, Iss. 9: 380 (2015); https://ijiset.com/vol2/v2s9/IJISET_V2_I9_47.pdf
15. C. K. Rhee, A. D. Maksimov, I. V. Beketov, A. O. Medvedev, and A. M. Murzkaev, *J. Korean Powder Metall. Inst.*, **27**, No. 6: 464 (2020); https://doi.org/10.4150/KPMI.2020.27.6.464
16. Kailun Zhang, Ruike Bi, Johan Tidholm, Jakob Angby, Mattias Richter, and Andreas Ehn, *Applied Spetroscopy*, **79**, Iss. 2: 281 (2025); https://doi.org/10.1177/00037028241285150
17. V. F. Tarasenko, *Runaway Electrons Preionized Diffuse Discharge* (New York: Nova Science Publishers Inc.: 2014).
18. R. Hrytsak, O. Minya, O. Shuaibov, and M. Feldii, *Proceedings of the 4th International Scientific and Practical Conference 'Recent Trends in Science' (May 8–9, 2025, Dnipro, Ukraine)*, p. 9–11.
19. G. A. Mesyats, *Physics–Uspekhi*, **38**, No. 6: 567 (1995); https://doi.org/10.3367/UFNr.0165.199506a.0601
20. O. K. Shuaibov and A. O. Malinina, *Progress in Physics of Metals*, **22**, No. 3: 382 (2021); https://doi.org/10.15407/ufm.22.03.382
21. *NIST Atomic Spectra Database Lines Form*; https://physics.nist.gov/PhysRefData/ASD/lines_form.html
22. A. R. Striganov, *Tables of Spectral Lines of Neutral and Ionized Atoms* (New York: Springer: 1968).
23. A. Omarov, V. S. Kurbanismailov, G. B. Ragimkhanov, M. Kh. Gadzhiev, and M. V. Kurbanismailov, *Bulletin of Dagestan University*, **6**: 5 (2012).
24. V. S. Kurbanismailov, O. A. Omarov, and G. B. Ragimkhanov, *Applied Physics*, **2**, No. 3: 35 (2014).
25. A. A. Radzig and B. M. Smirnov, *Reference Data on Atoms, Molecules, and Ions* (Heidelberg–Berlin: Springer: 1985).
26. G. J. M. Hagelaar, *Plasma Sources Sci. Techn.*, **14**, No. 4: 722 (2005); https://doi.org/10.1088/0963-0252/14/4/011
27. *BOLSIG+, Electron Boltzmann Equation Solver* [Electronic resource]: http://www.bolsig.laplace.univ-tlse.fr/
28. Yu. M. Smirnov, *Journal of Applied Spectroscopy*, **76**, No. 5: 611 (2009); https://doi.org/10.1007/s10812-009-9262-3
29. https://www-amdis.iaea.org/ALADDIN
30. Yu. P. Raizer, *Gas Discharge Physics* (Berlin–Heidelberg: Springer: 1991).